

1
2
3
4
5
6
7
8
9
10
11
12
13
14
15
16
17
18
19
20
21
22
23
24
25
26
27
28
29
30
31

Electronic Supplementary Information

Controlling the distance of highly confined droplets in a capillary by interfacial tension for merging on-demand

D. Ferraro^a, M. Serra^{b,c}, D. Filippi^a, L. Zago^a, E. Guglielmin^a, M. Pierno^a, S. Descroix^{b,c}, J.-L. Viovy^{b,c,*}, G. Mistura^{a,*}

^a Dipartimento di Fisica e Astronomia G. Galilei, Università di Padova, via Marzolo 8, 35131 Padova, Italy

^b Laboratoire Physico Chimie Curie, Institut Curie, PSL Research University, CNRS UMR168, Paris, France

^c Institut Pierre-Gilles de Gennes, Paris, France

*email: Giampaolo Mistura (giampaolo.mistura@unipd.it); Jean-Louis Viovy (jean-louis.viovy@curie.fr)

1. Characterization of the oil phase FC40+PEG-Krytox

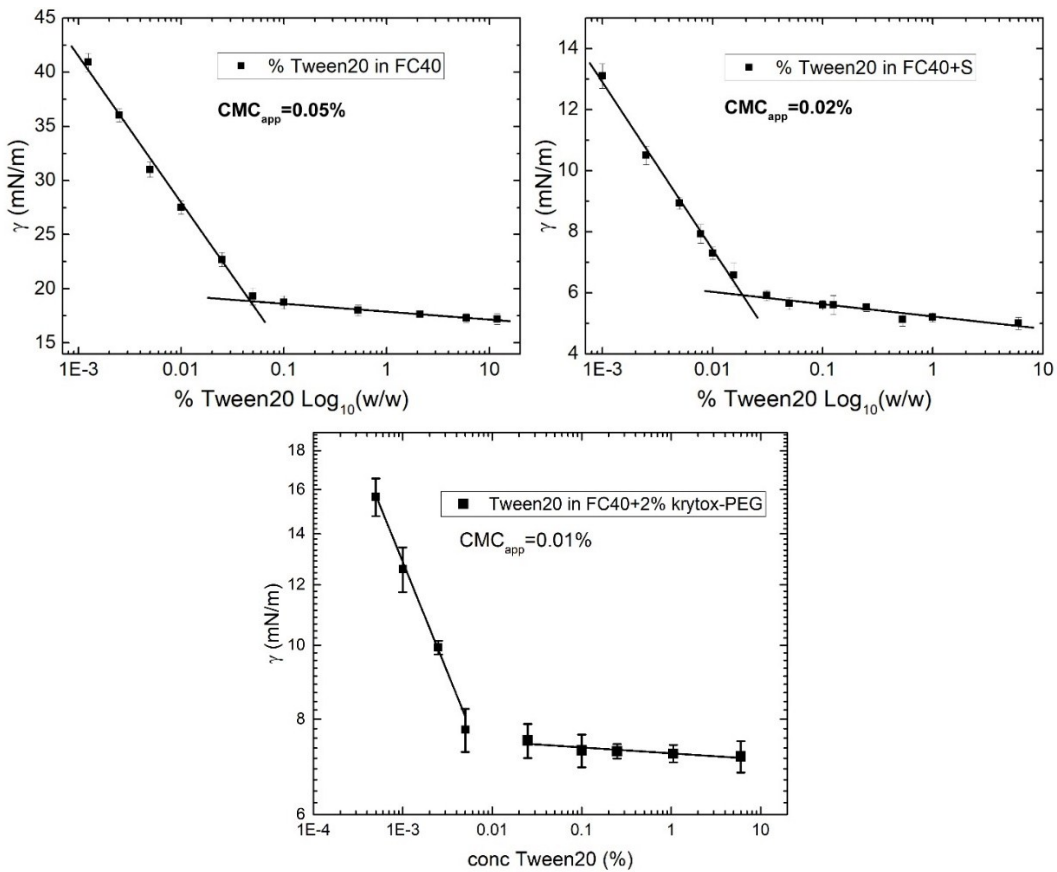
The table S1 reports the interfacial tension (γ) and viscosity ratio (λ) between the water phase (droplet phase) and the FC40 mixed with 2% of PEG-Krytox surfactant (PK). All dilutions are measured as wt%.

Table S1. List of the liquids properties used as continuous and dispersed phases during the experiments with the Krytox-PEG surfactant (PK) in the continuous phase.

FC40 + PK (viscosity: 4.28±0.05mPa·s)		
Dispersed phase	γ (mN/m)	λ
milliQ water	18.87±1.2	0.241±0.004
EtOH 4%	15.1±0.6	0.277±0.004
EtOH 8%	11.4±0.5	0.411±0.004
EtOH 15%	9.0±0.3	0.510±0.004
EtOH 31%	5.5±0.1	0.510±0.004
Tween20 - 0.0001%	15.7±0.9	0.239±0.004
Tween20 - 0.001%	12.6±0.8	0.239±0.004
Tween20 - 0.0025%	9.9±0.2	0.239±0.004
Tween20 - 0.0005%	7.7±0.5	0.240±0.004
Tween20 - 0.025%	7.5±0.4	0.247±0.004
Tween20 - 0.1%	7.2±0.3	0.247±0.004
Tween20 - 0.25%	7.2±0.2	0.247±0.004
Tween20 - 1%	7.1±0.2	0.247±0.004
Tween20 - 6%	7.1±0.3	0.249±0.004

32 2. Measurement of the apparent Critical Micelle Concentration (CMC_{app})

33 The apparent Critical Micelle Concentration (CMC_{app}) of the Tween20 surfactant dissolved in milliQ-water
34 with FC40 oil was measured in three conditions: (a) pure oil, (b) oil mixed with 2% (wt.) of 1H, 1H, 2H, 2H-
35 perfluoro-1-decanol (FC40+PFD) and (c) oil mixed with 2% (wt.) of Krytox-PEG (FC40+KP). The graphs
36 reported in Figure S1 show the interfacial tension γ measured with the pendant drop method as a function
37 of the concentration of Tween20 in water (plotted in logarithmic scale). As conventionally done¹, for each
38 graph the two groups of data are fitted by two independent straight lines and the CMC_{app} is evaluated as their
39 intersections. The resulting CMC_{app} values are 0.05%, 0.02% and 0.01% in (a) FC40, (b) FC40+PFD and
40 FC40+KP case, respectively.



41

42

43 **Figure S1.** Evaluation of the CMC_{app} of the water phase mixed with Tween20 at different concentration, with the three
44 used oil phases: (a) FC40, (b) FC40+PFD and (c) FC40+KP.

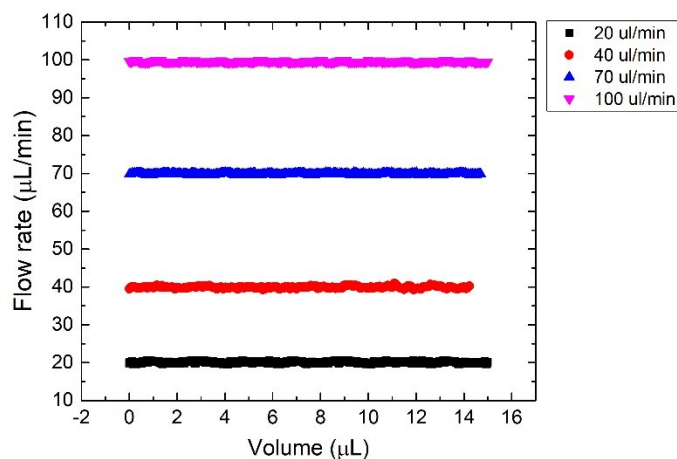
45

46

47

48 3. Evaluation of the stability of the flow generated by the syringe pump.

49 Flow rates generated by a syringe pump may be affected to oscillations due to the mechanical actuation
50 system. We have monitored the stability of the flows by connecting the syringe in series to a flowmeter (type
51 L, by Fluigent). Figure S2 reports the measured values as a function of the total volume flown through the
52 sensor. Table S2 summarizes the measured mean values together with the maxima and minima. It clearly
53 shows that the flow oscillations generated by the syringe pump system are always less than 1%. This
54 observation is also confirmed by the fact that the droplets exhibit a reproducible constant speed (see Figure
55 1e of the manuscript).



56
57 **Figure S2.** Flow rate generated by the setup described in Figure 1 (main paper) as a function of the pumped volume,
58 for different nominal flow-rates imposed.

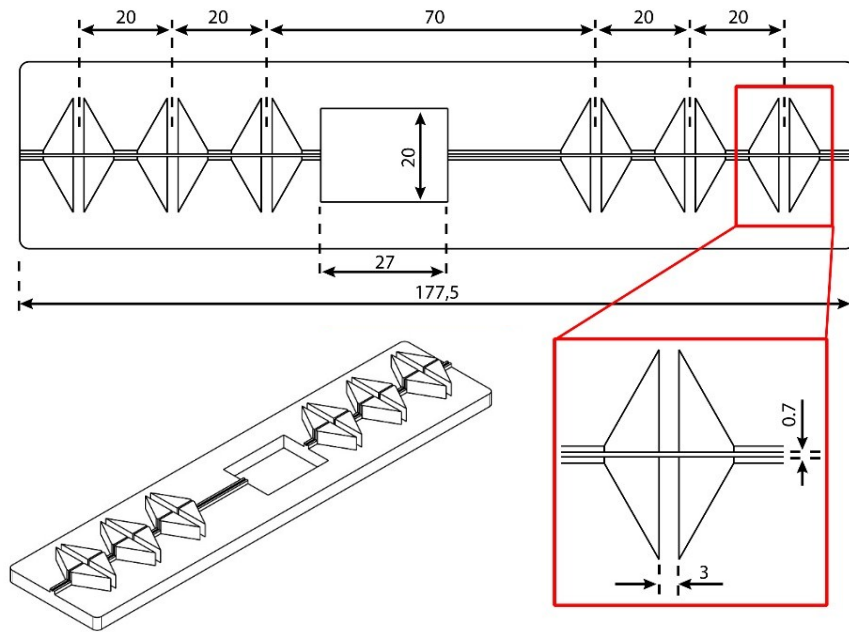
59
60 **Table S2.** Average values and statistics obtained from the data plotted in Figure S2.

Nominal Imposed Flow rate	Measured Flow rate (mean)	err %	Max Value	Min Value
µL/min	µL/min		µL/min	µL/min
20	20.07±0.21	1.0%	20.57	19.58
40	39.93±0.27	0.7%	40.96	39.25
70	69.89±0.17	0.2%	70.23	69.64
100	99.85±0.17	0.2%	100.07	99.58

61
62
63

64 **4. Optical Fibers and capillary holder**

65 In order to accurately position and fix the optical fibers in correspondence of the capillary transporting the
66 droplets, we designed a 3D printed structure, adapted to the dimensions of the used components. Figure S3
67 shows the sketch of the 3D part, in which 6 pairs of fibers (3mm diameters) can be hosted at specific
68 distances. The rectangular through hole present in the center of the structure provides an observation
69 window for the image acquisition by the microscope (see Materials and Methods in the main text).



70

71

72 **Figure S3.** Sketch of the 3D part used as holder for the optical fibers and the capillary.

73

74 **5. Evaluation of the correct oil speed U**

75 The normalized droplet speed β is calculated as the ratio between the droplet speed V and the carrier oil
76 speed U . While V is directly measured by the experimental setup 1 (see Materials and Methods), U
77 is calculated as $U = \phi / \pi r^2$, where ϕ is the flow rate set by the syringe pump and r is the radius of the capillary.
78 In order to properly evaluate U , we have performed direct measurements of both ϕ and r . The flow-rate
79 control of the syringe pump depends exclusively on the nominal diameter of the used syringe and does not
80 include any feed-back control on the generated flow. Therefore, before starting the experiments, we directly
81 measured the volume of FC40 oil flowed in a known amount of time, by weighting the liquid using a
82 microbalance. We repeated the measurements at least 10 times for each investigated flow-rate, considering
83 different volumes in the working range (from 5 to 50 μ L). The averaged results are reported in Table S3 and
84 the discrepancy with the nominal values was found to be less than 1% for the investigated flow-rates
85 (between 20 and 100 μ L/min).

86 After that, in order to obtain an experimental value for r , we measured the capillary diameters d by optical
87 microscopy. In order to reduce the aberrations due to its circular cross section, the capillary was pre-filled
88 with water and immersed in fluorinated oil (see Figure S4). More than 30 measures were performed along
89 the tube length (about 35 cm). The average radius was found to be $r = 145 \pm 1 \mu$ m and was used for the β
90 calculation.

91

92

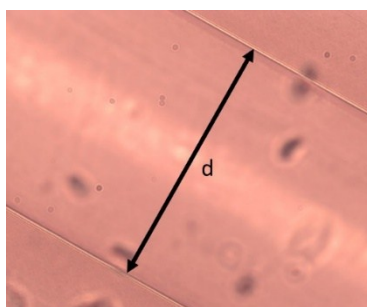
93

94

95 **Table S3.** Discrepancy between nominal and measured flow rate applied by the syringe pump.

nominal flow rate ($\mu\text{L}/\text{min}$)	measured flow rate ($\mu\text{L}/\text{min}$)	% variation
20	20.07 ± 0.04	0.3%
30	30.19 ± 0.08	0.6%
40	40.24 ± 0.11	0.6%
55	55.38 ± 0.07	0.7%
70	70.40 ± 0.17	0.6%
100	100.75 ± 0.34	0.7%

96



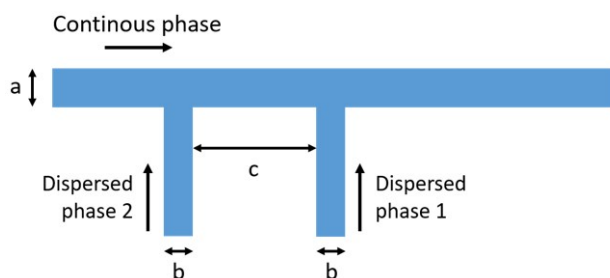
97

98 **Figure S4.** Microscope image of the capillary for the experimental measurement of its diameter d . The capillary diameter
99 is evaluated using ImageJ software.

100

101 **6. Scheme of the microfluidic device used in the setup 2, for droplet on demand generation**

102 The microfluidic PDMS device, integrated in Setup 2, is characterized by two consecutive T-junction
103 geometries (see Scheme in Fig. S5). This design allows the production of droplet pairs, containing different
104 water phase-solutions, transported by a carrier FC-40 oil. Furthermore, a customized pinch-like microvalve
105 set-up controls each inlet for on-demand droplet generation². It is then possible to generate sequences of
106 droplet pairs of arbitrary volumes and spaced by a customized oil gap, allowing thus to precisely span a wide
107 range of conditions.

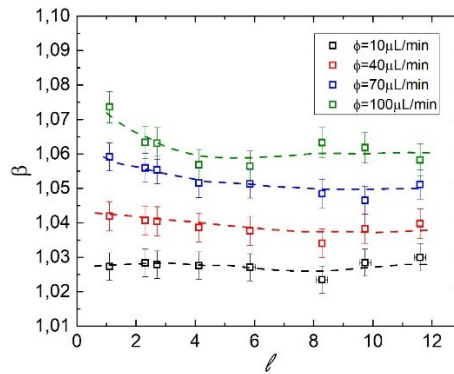


108

109 **Fig S5.** Geometrical scheme of the microfluidic device used for droplet-on-demand generation. Channel widths are the
110 following: $a=400\mu\text{m}$, $b=200\mu\text{m}$, $c=6.8\text{mm}$. The channel thickness is constant along all the device and equal to $200\mu\text{m}$.

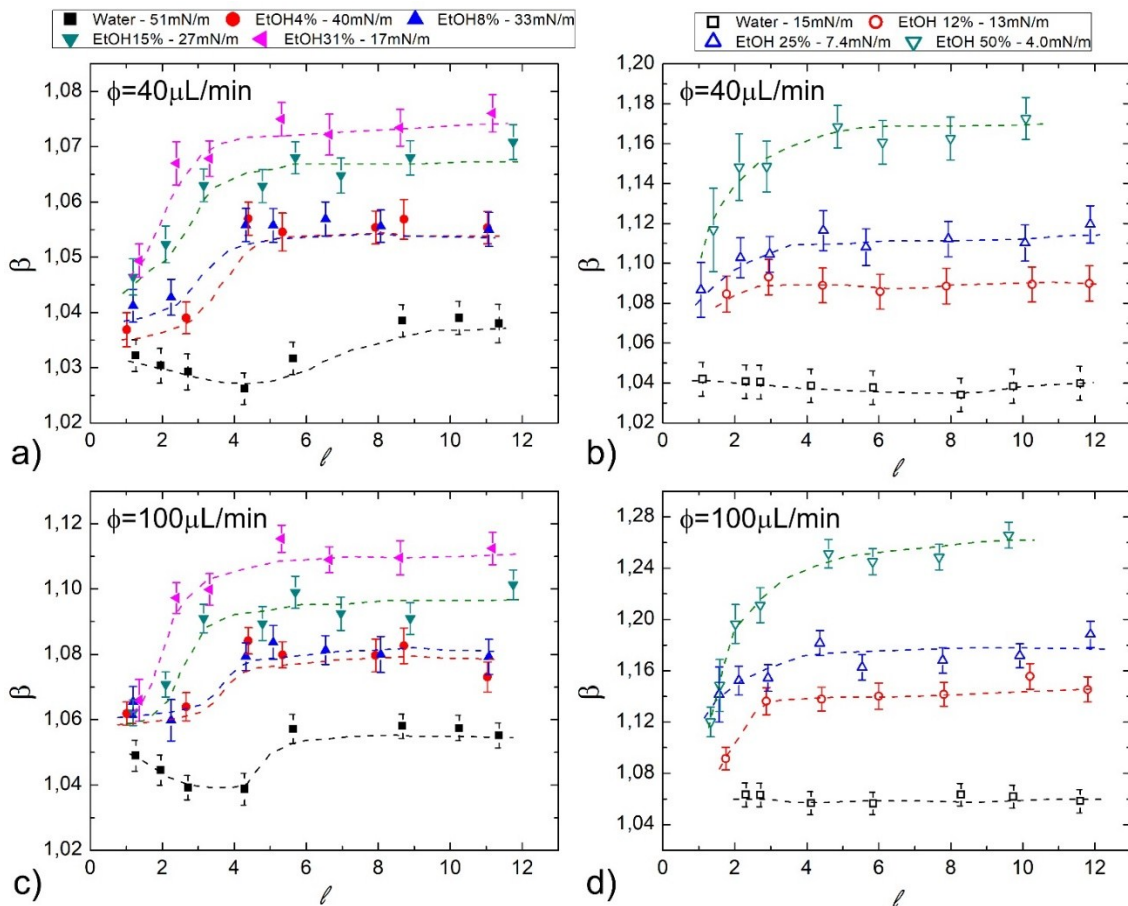
111 **7. Influence of the normalized droplet length l on the droplet mobility β**

112 The behavior of β against l was investigated in different conditions, as reported in the graphs below. These
 113 data integrate the ones presented in the main text. In details, Figure S6, which completes the results
 114 presented in Figure 3 of the paper, describes the results for pure water droplets transported by FC40+S. In
 115 addition, Figures S7 and S8 extends the results presented in Figures 4 and 5 of the main text, considering
 116 different flow-rates values ($40\mu\text{L}/\text{min}$ and $100\mu\text{L}/\text{min}$, respectively).



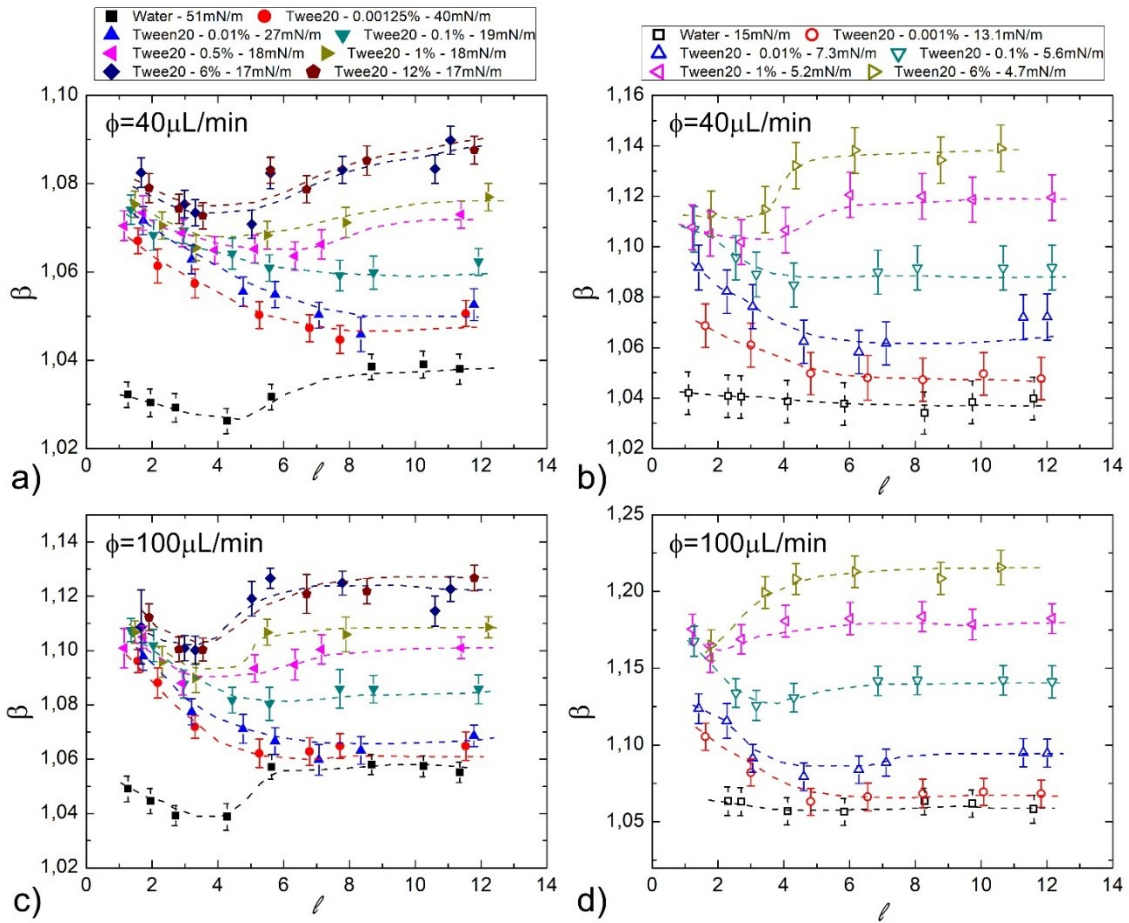
117

118 **Fig S6.** Normalized droplet speed β as function of the normalized droplet length l using pure water as dispersed phase
 119 and pure FC40+S as continuous phase, for different flow rates ϕ , which acts shifting the data along the Y axis.
 120



121

122 **Fig S7.** Normalized droplet speed β as function of the normalized droplet length l using ethanol-water solutions as
 123 dispersed phase. (a,c) FC40 and (b,d) FC40+S are used as continuous phases in two flow rate conditions: (a,b)
 124 $\phi=40\mu\text{L}/\text{min}$ and (c,d) $\phi=100\mu\text{L}/\text{min}$.
 125



126

127 **Fig S8.** Normalized droplet speed β as a function of the normalized droplet length l using Tween20 in water as dispersed
 128 phase. (a,c) FC40 and (b,d) FC40+S are used as continuous phases in two flow rate conditions: (a,b) $\phi=40\mu\text{L}/\text{min}$ and
 129 (c,d) $\phi=100\mu\text{L}/\text{min}$.

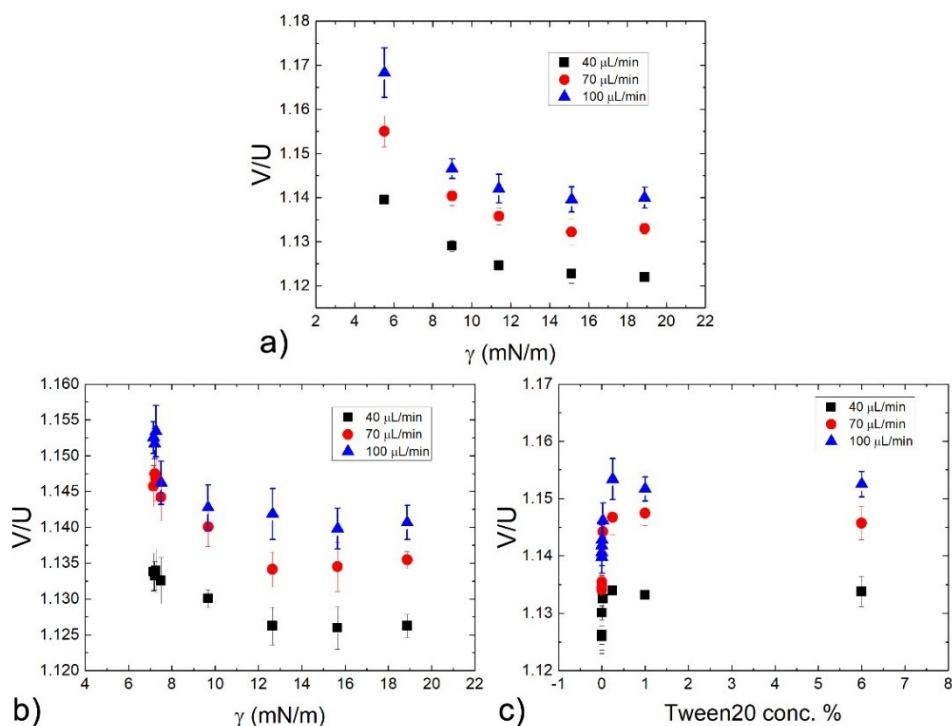
130

131

132

133 8. Evaluation of the normalized droplet speed using the PK surfactant in the continuous phase.

134 Considering the large diffusion of the Krytox-PEG surfactant, we report in Figure S9 the normalized droplet
135 speed as a function of the interfacial tension using water mixtures of (a) ethanol and (b) Tween20 as
136 dispersed phases. For the latter case, we also plot the same data as a function of the Tween20 concentration
137 (c). The data trends are similar to those observed in the case of PFD surfactants in the oil phase: the droplet
138 speed increases at low γ . Finally, the reported graphs indicate that once the flow rate of the carrier fluid is
139 fixed, decreasing γ by one order of magnitude causes a variation in the droplet speed of about 2-3%.
140 Therefore, even if the general trends are similar to the case of PFD, the speed variation is much smaller,
141 probably due to the different type of surfactant dispersed in the oil phase.



142 **Figure S9.** Normalized speed of droplet containing (a) ethanol-water mix and (b) Tween20 in FC40 with 2% of Krytox-
143 PEG surfactant. (c) Normalized speed of droplet as function of the Tween20 concentration in the droplet.

145

146 9. Supplementary movies: the on-demand merging approach

147 **Movie S1.** Example of the measurement of the distance traveled by the droplets from their generation to the
148 merging point (ΔS_m) by using the setup 2. Sequences of droplets pairs generated with a fixed initial oil gap
149 distance (ΔS_i) merge in a specific and reproducible position. The first and second droplets contain pure water
150 and water phase with 1% of Tween20, respectively. Red food coloring dye is added in both droplet solutions
151 to help their observation.

152

153 **Movie S2, S3, S4.** Pairs of droplets flowing in the circular capillary containing pure water and Tween 1%,
154 respectively. Although they are generated with an identical initial distance ($\Delta S_i \approx 10\text{mm}$), the droplets merge
155 at different positions depending on the flow rate ϕ of the continuous phase (S2: 30 $\mu\text{L}/\text{min}$, S3: 50 $\mu\text{L}/\text{min}$, S4:
156 100 $\mu\text{L}/\text{min}$). This shows that higher ϕ leads to an earlier merging. Red food coloring dye is added in both the
157 droplet solutions to help their observation.

158

159 Reference

160 1 E. C. Wijaya, F. Separovic, C. J. Drummond and T. L. Greaves, *Phys. Chem. Chem. Phys.*, 2016, **18**,
161 24377–24386.

162 2 D. Ferraro, M. Serra, I. Ferrante, J.-L. Viovy and S. Descroix, *Sensors Actuators B Chem.*, 2018, **258**,
163 1051–1059.